Structural States and Dynamics of the D-Loop in Actin

Zeynep A. Oztug Durer,[†] Dmitri S. Kudryashov,[†] Michael R. Sawaya,[†¶] Christian Altenbach,[†§] Wayne Hubbell,[†‡§] and Emil Reisler[†‡]

[†]Department of Chemistry and Biochemistry, [‡]Molecular Biology Institute, [§]Jules Stein Eye Institute, and [¶]UCLA-DOE Institute for Genomics and Proteomics, University of California, Los Angeles, California

Supporting Material

Methods

Actin cycling

Mutant actins were first polymerized with 3.0 mM $MgCl_2$ and then pelleted by centrifugation at 375,000 g for 20 minutes, at 4°C, in a Beckman TLA-110 rotor. The resulting pellet was soaked in half of the starting volume of buffer B [5.0 mM Tris (pH 8.0), 1 mM DTT, 0.2 mM ATP, and 0.2 mM $CaCl_2$] for 45-60 minutes, and subsequently homogenized by vigorous pipetting and dialyzed overnight against 1L of buffer B. Next day, the dialyzed actin was centrifuged at 375,000 g for 20 minutes in a Beckman TLA-110 rotor to remove any polymerized protein. The resulting supernatant, containing Ca-G-actin, was used in the acrylodan labeling experiments.

GS1-Cobl fusion protein construction, purification, and crystallization.

DNA encoding a fusion protein of human gelsolin segment 1 (GS1; residues residues 52-174 from plasma gelsolin with an accession number P06396) with mouse WH2 tandem domains of Cobl (residues 1201-1337) followed by the pointed-end capping helix from thymosin beta-4 (residues 21-44) was constructed by PCR. The resulted sequence was cloned into pCOLD-I vector (Takara) in between NdeI and BamH1 restriction sites using In-fusion PCR cloning system (Clontech). The encoded protein contains the 6-His tag and Factor-Xa cleavage sequences (MNHKVHHHHHHIEGRHMGS) N-terminally to the GS1 sequence. The chimera protein was expressed in MMI medium at 15^{o}C overnight in Rosetta-2 cells (Novagen) and purified by metal chelate chromatography on Ni-NTA column (Qiagen). The fractions containing a mixture of the full length construct (apparent molecular weight on SDS PAGE ~38 kDa) and a product of its proteolytic degradation (apparent molecular weight on SDS PAGE ~34 kDa) were pooled together, dialyzed, mixed with excess of α-skeletal G-actin and separated by size exclusion chromatography on Superdex 75 column (Amersham Biosciences). Fractions containing actin and the 34 kDa protein were purified to homogeneity and used for crystallization. The crystallization trays were set using Mosquito

crystallization robot, with 2 µl drops containing a 1:1, 1:2, and 2:1 (v/v) mixture of protein solution and precipitant. Crystals were obtained in precipitant solution of 10% (w/v) polyethyleneglycol 20000, 2% (v/v) dioxane, and 0.1 M Bicine, pH 9.0, typically overnight.

X-Ray Data Collection.

X-ray diffraction data were collected at the Advanced Photon Source beamline 24-ID-C using an ADSC Quantum 315 3X3 CCD array. Crystals were cryo-cooled to 100 K for data collection. One hundred-eighteen 1.0° oscillation frames were collected at a wavelength of 0.9794 Å. Data reduction and scaling were performed using DENZO/SCALEPACK (1). Diffraction extending to 3.0 Å resolution was observed.

Structure determination and refinement.

The structure was solved using molecular replacement methods implemented by the program PHASER (2) and the crystal structure of the actin-GSI complex (PDB code 3CJB) (3) as a search model. Refinement was performed first with REFMAC5 (4) using TLS parameterization of domain disorder (5). After each refinement step, the model was visually inspected in Coot (6), using both 2Fo-Fc and Fo-Fc difference maps. The model was validated with the following structure validation tools: PROCHECK (7), ERRAT (8), and VERIFY3D (9). All of the residues are within the most favoured and additional allowed regions of the Ramachandran plot except for one residue (actin Ser232) in the generously allowed regions. The Errat score, 95.5%, indicates that this percentage of residues has a calculated error value that falls below the 95% rejection limit. The coordinates of the final model and the merged structure factors were deposited with the Protein Data Bank with the corresponding PDB ID: 3TU5. Figures were illustrated using Pymol (De Lano, 2002, DeLano Scientific, San Carlos, CA, USA).

Representing D-loop conformers in current F-actin models - creation of hybrid structural coordinates

The calculation of the expected SASA and pKa parameters of the D-loop cysteines in extended (3MFP, and 2ZWH), helical (1J6Z), and hairpin (1YAG and 3TU5) D-loop conformations in the Oda et al. (10) or Fujii et al. (11) model coordinates, involved three steps. First the structure files were created by aligning the subdomain 2 (residues 31-69) regions of several actin monomers taken from crystal structures (PDB IDs 1YAG, 1J6Z, 3TU5, and the protomers of 3MFP and 2ZWH) with the actin model of interest (PDB IDs 3MFP and 2ZWH). In the second step, once the alignment was performed in PYMOL, the original subdomain 2 of the model used was deleted, allowing the creation of hybrid models with distinct conformers of D-loop. In the third step, these hybrid model coordinates were subjected to cysteine mutagenesis using PYMOL's mutagenesis tool, with the most probable rotamer considered to be the one with the least amount of steric hindrance. The mutations on Holmes 2003 model (12) were based directly on the original pdb file of that model.

Supporting Tables

Table S1. Data collection and refinement statistics for actin-GS1-Cobl structure

	actin-GS1-Cobl
Data collection	
Space group	$P3_221$
Cell dimensions□□	
a, *b*, *c* (Å)	71.2, 71.2, 222.2
Resolution (Å)	3.0 (3.1-3. 0)
R_{sym}	0.089 (0.493)
$I/\sigma I$	19.2 (4.8)
Completeness (%)	96.3 (98.1)
Redundancy	7.0 (7.2)
Refinement	
Resolution (Å)	3.0
No. reflections	13297
$R_{work/}$ R_{free}	0.165/0.205
No. atoms	
Protein	3943
Ligand/ion	49
Water	65
B-factors (Å^2)	
Protein	74.7
Ligand/ion	59.7
R.m.s deviations	
Bond lengths (Å)	0.010
Bond angles (º)	1.1

*Highest resolution shell is shown in parenthesis.

Table S2. Rotational correlation times, τ_c, of the R1 probe on Ca-G-actin mutants

Residue Number	Component 1		Component 2	
	τ_{c1} (ns)	%	τ_{c2} (ns)	%
C40	**1.2**	100		
C41	**1.1**	78	**3.2**	24
C43	**0.9**	74	**2.5**	25
C45	**0.9**	66	**2.7**	33
C46	**0.8**	68	**2.8**	29
C47	**0.7**	63	**2.5**	34
C48	**0.9**	64	**3.2**	20
C49	**1.3**	71	**3.5**	31
C50	**1.3**	100		

τ_c and the relative amounts of each component were determined from the simulations of EPR spectra, as described in Materials and Methods. For EPR spectra of mutants C40 and C50, the second component did not improve the fit. Percentage columns present the relative populations of R1 with τ_{c1} and τ_{c2} correlation times.

Table S3. Fluorescence properties of acrylodan conjugated cysteine mutants

Probed residues	λ_{max} emission (nm)			Ratio of F_{max}
D-loop	**G-actin**	**F-actin**	**F-actin + Ph**	**(F-actin+Ph)/G-actin**
C40	511	-	496	1.7
C41	518	509	508	1.4
C42	514	508	506	1.4
C43	521	483	485	1.9
C45	516	497	497	1.5
C46	517	499	500	1.8
C47	518	503	504	1.9
C48	520	490	488	1.9
C49	519	514	513	1.5
C50	516	513	512	1.5

Fluorescence emission maxima, λ_{max}, are given for Ca-ATP-G, Mg-ADP-F, and phalloidin stabilized Mg-ADP-F actins. The last column lists ratios of maximum fluorescence of F-actin over that of G-actin.

Table S4. Normalized SASA(%) of D-loop cysteines in G-actin based on the available actin structures.

Res. #	Hairpin-1YAG	Helical-1J6Z	Hairpins-3TU5	Loop-2ZWH	Loop-3MFP
40	75	48	67	58	87
41	52	69	60	74	61
42	37	67	53	75	72
43	92	41	100	27	71
44	53	11	74	63	65
45	87	40	29	93	94
46	85	83	42	84	72
47	46	42	80	57	94
48	2	69	95	45	99
49	47	62	64	68	46
50	40	42	55	28	35

Solvent accessible areas of D-loop cysteines are calculated with CCP4i as described in Materials and Methods. All SASA values were normalized to the highest accessible area of C43 in 3TU5, which was 141.7 $Å^2$. Column headers indicate the conformation observed for D-loop in a given structure and the PDB ID for that structure.

Table S5. pKa values of D-loop cysteines in G-actin based on current actin models and structures.

Res. #	Hairpin-1YAG	Helical-1J6Z	Hairpins-3TU5	Loop-2ZWH	Loop-3MFP
40	9.0	5.0	9.0	9.0	9.0
41	9.2	8.8	9.2	8.3	6.7
42	8.9	8.9	6.5	7.7	9.1
43	9.0	8.6	8.4	7.5	8.3
44	8.7	9.1	9.0	9.0	7.6
45	9.0	7.9	9.1	9.0	9.0
46	9.1	8.8	9.1	9.0	9.0
47	8.4	9.1	8.5	7.5	8.6
48	8.8	9.1	9.0	9.0	7.9
49	8.3	9.0	9.0	7.7	9.0
50	8.5	9.0	8.4	9.7	8.7

pKa values were predicted by PROPKA software as described in Materials and Methods. The reported standard deviation is 1 pKa unit. Column headers indicate the conformation observed for D-loop in a given structure and the PDB ID for that structure.

Table S6. Normalized SASA (%) of D-loop cysteines in F-actin based on the current actin models and structures.

Res #	Loop-ODA	Helical-ODA	Helical-HOLMES	Helical-FUJII	Loop-FUJII	Hairpins-ODA-3TU5	Hairpin-Oda-1YAG	Exp. Reac.
40	14	29	34	21	43	30	38	195
41	61	69	69	69	59	60	49	163
42	28	31	50	48	36	53	16	192
43	41	8	3	3	55	100	74	100
44	50	11	11	11	34	49	19	—
45	40	40	11	40	45	23	64	279
46	29	18	18	32	40	19	32	526
47	48	17	16	22	91	63	0	100
48	1	67	45	69	99	83	1	279
49	68	62	44	59	40	51	47	68
50	28	42	43	42	35	55	40	47

Solvent accessible areas of D-loop cysteines are calculated with CCP4i as described in Materials and Methods. All SASA values were normalized to the highest accessible area of C43 (in 3TU5), which was 141.7 $Å^2$. Column headers indicate D-loop conformation in a given structure and the corresponding PDB ID. The last column lists the experimentally determined modification rates of F-actin normalized to the rate constant observed for C43.

Table S7. pKa values of D-loop cysteines in F-actin based on current actin models and structures.

Res #	Loop-ODA	Helical-ODA	Helical-HOLMES	Helical-FUJII	Loop-FUJII	Hairpins-ODA-3TU5	Hairpin-Oda-1YAG	Exp. Reac.
40	10.8	5.6	5.5	4.8	8.8	9.7	9.1	195
41	7.5	8.8	8.8	8.8	6.7	9.2	9.2	163
42	7.5	4.4	4.0	4.2	8.6	6.5	9.2	192
43	8.2	5.6	4.6	5.0	8.9	8.4	9.0	100
44	9.0	9.1	9.1	9.1	7.7	9.0	8.3	—
45	9.4	7.9	7.9	7.9	9.4	9.4	9.0	279
46	8.8	9.1	7.4	9.7	8.9	7.5	7.6	526
47	7.5	9.1	9.4	9.1	8.6	8.5	8.6	100
48	9.2	9.1	6.2	9.1	7.9	9.0	9.0	279
49	7.7	9.0	9.1	9.0	9.0	9.0	8.3	68
50	9.7	9.0	9.0	9.0	8.7	8.4	8.5	47

The pKa values were predicted by PROPKA software as described in Materials and Methods. The reported standard deviation is 1 pKa unit. Column headers indicate D-loop conformation in a given structure and the corresponding PDB ID. The last column lists the experimentally determined modification rates of F-actin normalized to the rate constant observed for C43.

Table S8. Ratios of cysteine modification rates in G- and F-actins

Residue number	**C40**	**C41**	**C42**	**C43**	**C45**	**C46**	**C47**	**C48**	**C49**	**C50**
Modification rate ratio G/F	4.6	2.0	2.1	4.5	1.5	0.7	2.2	1.4	3.0	3.0

The rate constants for acrylodan modification observed in G-actins is divided by that for F-actins, to assess site specific reactivity changes upon filament formation.

Supporting Figures

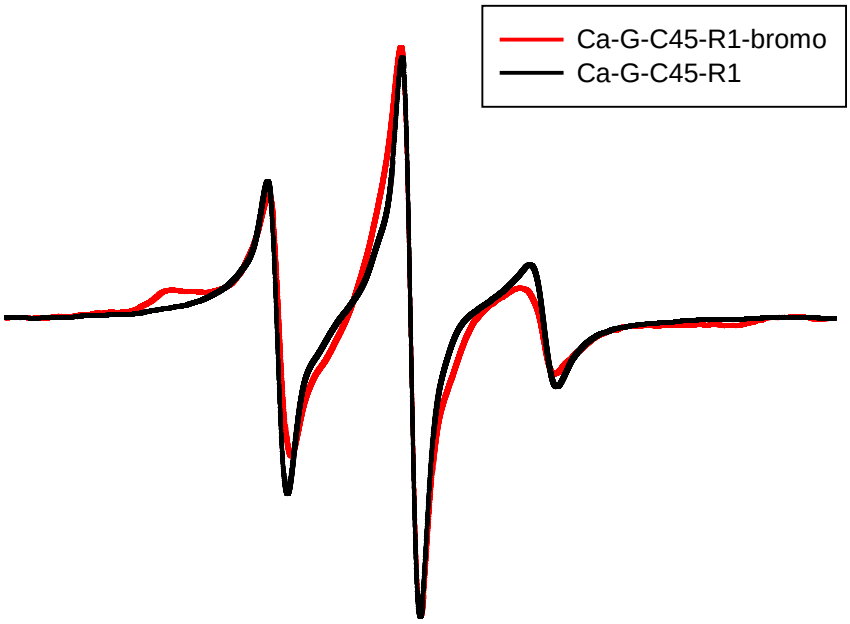

Fig.S1. EPR spectra of R1 (black line) and 4-bromo derivative of R1 (red line) labeled C45 yeast actin in the Ca-ATP-G-actin form. The R1-bromo spectrum is scaled up to the EPR central line height of Ca-G-C45-R1. The scan width is 100 Gauss.

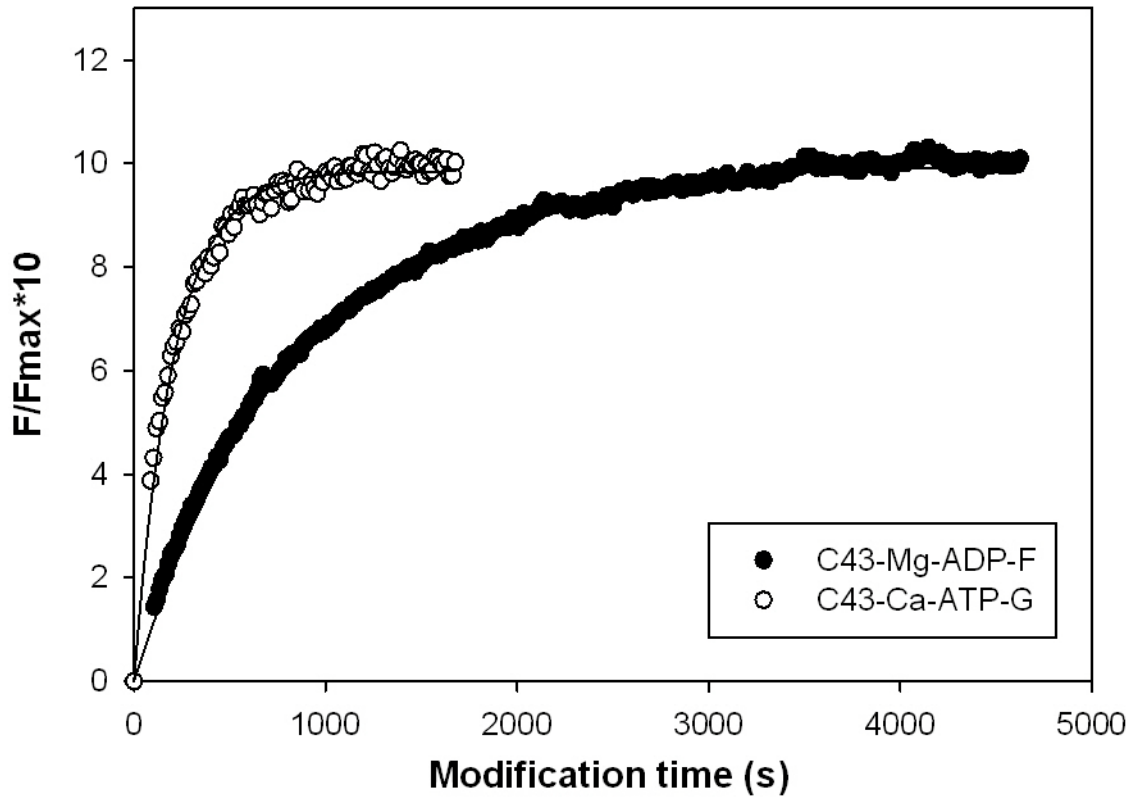

Fig.S2. Representative plot of acrylodan labeling of a D-loop cysteine mutant actin. Modification of C43 on actin by acrylodan was monitored via an increase in acrylodan fluorescence at 465 nm. The data were fitted to a single exponential, yielding a first order rate constant. The rate of C43 labeling was 4-fold higher in the monomer than in the polymer.

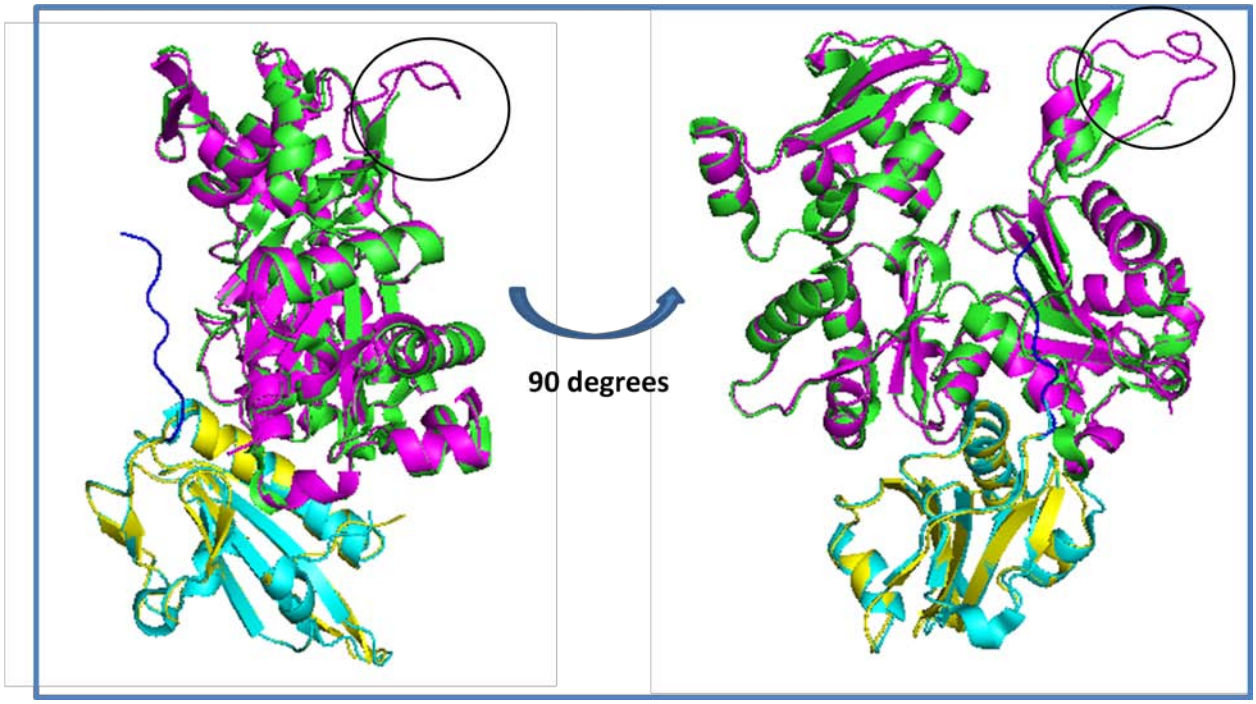

Fig.S3. Identification of a new D-loop conformer in a new crystal structure of actin-GS1-Cobl. Our actin-GS1-Cobl (PDB ID: 3TU5, actin in magenta, GS1 in yellow, and first 9 residues of Cobl in blue) is aligned with actin-GS1 (PDB ID: 1EQY, actin in green and GS1 in cyan) using PYMOL with 0.4 Å RMS. The sole difference between the two actin structures is in the presence of hairpins in the D-loop region of actin-GS1-Cobl (circled). Only the first 9 amino acids of Cobl WH2 domains are visible (due to proteolytic cleavage of Cobl during crystallization and/or due to crystallographic disorder).

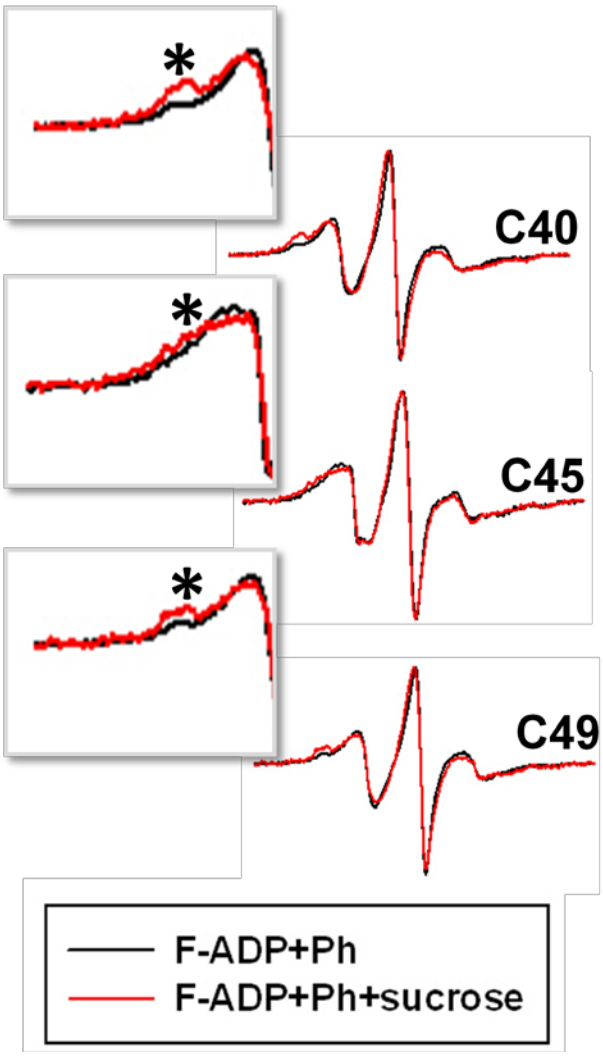

Fig.S4. EPR spectra of selected R1 labeled D-loop mutants in phalloidin stabilized Mg-ADP-F actin in the presence of 1M sucrose (red traces) or without sucrose (black traces). In each pair, the F-actin sucrose spectrum is scaled up to the EPR central line height of F-actin spectrum. The regions of EPR spectra most sensitive to the presence of sucrose are indicated by stars in the insets. The scan width is 100 Gauss.

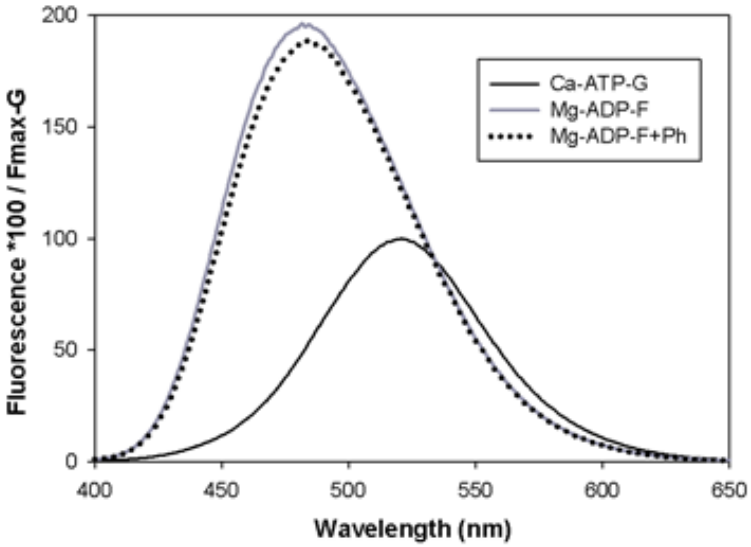

Fig.S5. Representative fluorescence emission spectrum of acrylodan labeled C43 actin. Fluorescence spectra of acrylodan-labeled C43 yeast actin was recorded for Ca-ATP-G (black solid line), Mg-ADP-F (gray solid line), and Mg-ADP-F actin in the presence of phalloidin (black dotted line).

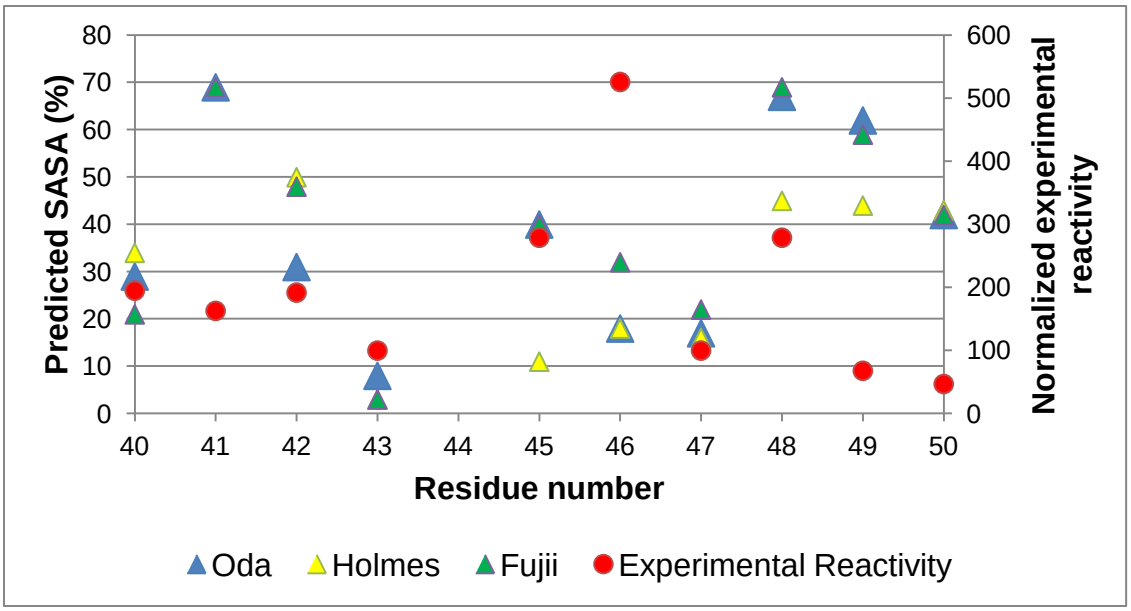

Fig.S6. Comparison of the trends of experimental reactivity values deduced from the label incorporation rates and the trends of predicted SASA values for current actin models incorporating a helical D-loop. Solvent accessible areas of D-loop cysteines are calculated with CCP4i as described in Materials and Methods considering a helical D-loop in Oda (10), Holmes (12), and Fujii (11) models of the actin filaments.

Supporting References

1. Otwinowski, Z., and W. Minor. 1997. Processing of X-ray Diffraction Data Collected in Oscillation Mode. In Macromolecular Crystallography, part A. C.W. Carter, Jr. & R. M. Sweet, Eds. 307-326.
2. McCoy, A. J., R. W. Grosse-Kunstleve, P. D. Adams, M. D. Winn, L. C. Storoni, and R. J. Read. 2007. Phaser crystallographic software. J Appl Crystallogr 40:658-674.
3. Kudryashov, D. S., Z. A. Durer, A. J. Ytterberg, M. R. Sawaya, I. Pashkov, K. Prochazkova, T. O. Yeates, R. R. Loo, J. A. Loo, K. J. Satchell, and E. Reisler. 2008. Connecting actin monomers by iso-peptide bond is a toxicity mechanism of the Vibrio cholerae MARTX toxin. Proc Natl Acad Sci U S A 105:18537-18542.
4. Murshudov, G. N., A. A. Vagin, and E. J. Dodson. 1997. Refinement of macromolecular structures by the maximum-likelihood method. Acta Crystallogr D Biol Crystallogr 53:240-255.
5. Winn, M. D., G. N. Murshudov, and M. Z. Papiz. 2003. Macromolecular TLS refinement in REFMAC at moderate resolutions. Methods Enzymol 374:300-321.
6. Emsley, P., and K. Cowtan. 2004. Coot: model-building tools for molecular graphics. Acta Crystallogr D Biol Crystallogr 60:2126-2132.
7. Laskowski, R. A., D. S. Moss, and J. M. Thornton. 1993. Main-chain bond lengths and bond angles in protein structures. J Mol Biol 231:1049-1067.

8. Colovos, C., and T. O. Yeates. 1993. Verification of protein structures: patterns of nonbonded atomic interactions. Protein Sci 2:1511-1519.
9. Luthy, R., J. U. Bowie, and D. Eisenberg. 1992. Assessment of protein models with three-dimensional profiles. Nature 356:83-85.
10. Oda, T., M. Iwasa, T. Aihara, Y. Maeda, and A. Narita. 2009. The nature of the globular- to fibrous-actin transition. Nature 457:441-445.
11. Fujii, T., A. H. Iwane, T. Yanagida, and K. Namba. 2010. Direct visualization of secondary structures of F-actin by electron cryomicroscopy. Nature 467:724-728.
12. Holmes, K. C., I. Angert, F. J. Kull, W. Jahn, and R. R. Schroder. 2003. Electron cryo-microscopy shows how strong binding of myosin to actin releases nucleotide. Nature 425:423-427.